Translational Oncology
www.transonc.com

Volume 10 Number xx Month 2017 pp. 744–751 744

Ultrasound Elastography of the Prostate Using an Unconstrained Modulus Reconstruction Technique: A Pilot Clinical Study

Seyed Reza Mousavi[*,†,‡,§,¶], Hassan Rivaz[#,], Gregory J. Czarnota[*,†,‡,§], Abbas Samani[¶,††,‡‡,§§] and Ali Sadeghi-Naini[*,†,‡,§]**

[*]Department of Medical Biophysics, University of Toronto, Toronto, Ontario M4N 3M5, Canada; [†]Physical Sciences, Sunnybrook Research Institute, Sunnybrook Health Sciences Centre, Toronto, Ontario M4N 3M5, Canada; [‡]Department of Radiation Oncology, Odette Cancer Research, Sunnybrook Health Sciences Centre, Toronto, Ontario M4N 3M5, Canada; [§]Department of Radiation Oncology, University of Toronto, Toronto, Ontario M4N 3M5, Canada; [¶]Department of Medical Biophysics, Western University, London, Ontario N6A 5C1, Canada; [#]Department of Electrical and Computer Engineering, Concordia University, Montreal, Quebec H4B 1R6, Canada; [**]PERFORM Centre, Concordia University, Montreal, Quebec H4B 1R6, Canada; [††]Department of Electrical and Computer Engineering, Western University, London, Ontario N6A 5B9, Canada; [‡‡]Graduate Program in Biomedical Engineering, Western University, London, Ontario N6A 5B9, Canada; [§§]Imaging Research Laboratories, Robarts Research Institute (RRI), London, Ontario, N6A 5K8, Canada

Abstract

A novel full-inversion-based technique for quantitative ultrasound elastography was investigated in a pilot clinical study on five patients for non-invasive detection and localization of prostate cancer and quantification of its extent. Conventional-frequency ultrasound images and radiofrequency (RF) data (~5 MHz) were collected during mechanical stimulation of the prostate using a transrectal ultrasound probe. Pre and post-compression RF data were used to construct the strain images. The Young's modulus (YM) images were subsequently reconstructed using the derived strain images and the stress distribution estimated iteratively using finite element (FE) analysis. Tumor regions determined based on the reconstructed YM images were compared to whole-mount histopathology images of radical prostatectomy specimens. Results indicated that tumors were significantly stiffer than the surrounding tissue, demonstrating a relative YM of 2.5 ± 0.8 compared to normal prostate tissue. The YM images had a good agreement with the histopathology images in terms of tumor location within the prostate. On average, 76% ± 28% of tumor regions detected based on the proposed method were inside respective tumor areas identified in the histopathology images. Results of a linear regression analysis demonstrated a good correlation between the disease extents estimated using the reconstructed YM images and those determined from whole-mount histopathology images (r^2 = 0.71). This pilot study demonstrates that the proposed method has a good potential for detection, localization and quantification of prostate cancer.

Address all correspondence to: Ali Sadeghi-Naini, Department of Medical Biophysics, University of Toronto, Sunnybrook Health Sciences Centre, 2075 Bayview Avenue, Room M6-605, Toronto, Ontario M4N 3M5.
E-mail: ali.sadeghi@sri.utoronto.ca
Received 3 April 2017; Revised 15 June 2017; Accepted 15 June 2017

1936-5233/17
http://dx.doi.org/10.1016/j.tranon.2017.06.006

The method can potentially be used for prostate needle biopsy guidance with the aim of decreasing the number of needle biopsies. The proposed technique utilizes conventional ultrasound imaging system only while no additional hardware attachment is required for mechanical stimulation or data acquisition. Therefore, the technique may be regarded as a non-invasive, low cost and potentially widely-available clinical tool for prostate cancer diagnosis.

Translational Oncology (2017) 10, 744–751

Introduction

Prostate cancer (PCa) is the most frequently diagnosed cancer and the third cause of cancer-related death in men (after lung and colorectal cancer) [1]. Similar to other types of cancer, early detection plays an important role in successful management of PCa. Studies have shown that the 5-year survival rate of prostate cancer associated with early diagnosis is almost 99% while this rate falls sharply to less than 28% for patients with late diagnosis [1]. To increase the chance of PCa detection at early stages periodic screening is recommended for men after the age of 50. In case of detecting suspicious abnormalities through screening, prostate needle biopsy is administered which is still considered as the clinical gold standard for PCa diagnosis [2]. Given that needle biopsy is invasive and is associated with issues including discomfort and infection, it is desirable to develop a non-invasive PCa diagnosis system that has high sensitivity and specificity for early detection while it can be potentially used for needle biopsy guidance to improve its outcome. Conventional PCa screening and detection techniques such as digital rectal examination (DRE) and prostate-specific antigen (PSA) testing are known to have inadequate sensitivity and specificity [3]. As such, imaging techniques based on low-cost and widely-available modalities that can improve the accuracy of prostate cancer detection is highly desirable for periodic clinical screening of PCa. Transrectal ultrasonography (TRUS) is an inexpensive, rapid and portable imaging modality that typically does not rely on injection of any exogenous contrast agent. PCa typically appear hypoechoic on TRUS. Since many hypoechoic regions found on TRUS are not cancer and many cancer cases are not hypoechoic [4,5], TRUS ability to detect and localize prostate cancer is limited. In an attempt to increase the sensitivity and specificity of TRUS, contrast-enhanced TRUS (CEUS) has been developed which measures tissue vascularisation using micro-bubbles as contrast agent. Recent studies have shown that CEUS is a promising technique for tumor localization [6]. However, clinical applications of microbubble agents remain limited due to difficulties in regulatory approval in many countries including the United States. A number of other methods process ultrasound backscattered radiofrequency (RF) signals to determine the bio-acoustic properties of the underlying tissue for characterizing its microstructure [7,8]. In this context, computer-aided TRUS frameworks, such as HistoScanning, were developed for PCa detection [9]. While initial results obtained using such techniques are promising, their application in routine clinical practice is still under evaluation [10–12].

To benefit from higher quality imaging modalities, a number of magnetic resonance imaging (MRI) techniques have been investigated for PCa assessment. The most common technique is the standard T2-weighted MR imaging which has demonstrated a relatively good sensitivity but low specificity in detecting PCa [13–15]. This method is not capable of accurate detection of cancer in the prostate's transitional zone while it suffers from significant intra-observer variability in PCa detection. Sensitivity and specificity of standard MR sequences can be improved in part using endorectal coils to increase the signal-to-noise ratio and quality of MR images. However, utilizing endorectal coil in MR imaging of the prostate is associated with patient discomfort and extra cost [16]. Functional and physiologic MR imaging techniques in conjunction with multi-parametric analysis demonstrated improvement in sensitivity and specificity of PCa detection [17]. Among these, MR spectroscopy imaging (MRSI) [18], Dynamic contrast-enhanced MRI (DCE-MRI) [19] and diffusion-weighted imaging (DWI) [20] are the most commonly used techniques. In particular, using these images in a multi-parametric MRI (mp-MRI) framework has demonstrated to improve tumor detection, localization and characterization, especially in the transitional zone [21,22]. The performance of mp-MRI is, however, still limited due to the intrinsic MR image limitations in visualizing prostate tumor regions [23] and inter-observer variability of tumor delineation [24].

Another imaging modality that has been applied for PCa assessment is positron emission tomography (PET). Whereas earlier studies showed that PET has limited sensitivity and specificity for PCa detection, capabilities of PET in PCA detection are still under investigation and several groups are examining new tracers to improve its accuracy in this context [25–27]. However, image resolution of PET images is poor (>5 mm); hence, it is suggested that PET be used in combination with other image modalities [27].

Given the complexity and variability of PCa pathologies, many research groups have been pursuing multimodality imaging approach as no single modality imaging technique has proven to be adequate [28]. While imaging additional tissue properties increases the chance of reliable PCa detection and diagnosis, selecting complementary characteristics should be done carefully, considering clinical acceptability and cost. Ultrasound (US) elastography or elasticity imaging, a method that utilizes local tissue stiffness as a contrast mechanism, can be considered for this purpose since it can be used near simultaneously with the low cost and widely available US imaging modality. The general concept of elastography has been used clinically for diagnostic purposes as alteration in tissue stiffness is frequently associated with pathology [29,30]. Several groups investigated US elastography techniques for prostate cancer detection and characterization [31–33], and for guiding needle biopsy procedure [34,35]. These techniques, however, are based on strain imaging. In strain imaging techniques, tissue strain images are generated using a set of ultrasound RF data acquired prior to and after a quasi-static mechanical stimulation to approximate the tissue elastic modulus distribution. Although strain imaging is suitable for real-time applications, it assumes a uniform stress distribution over the entire field of view. This stress uniformity assumption is invalid in the prostate imaging due to tissue heterogeneity and irregular geometry,

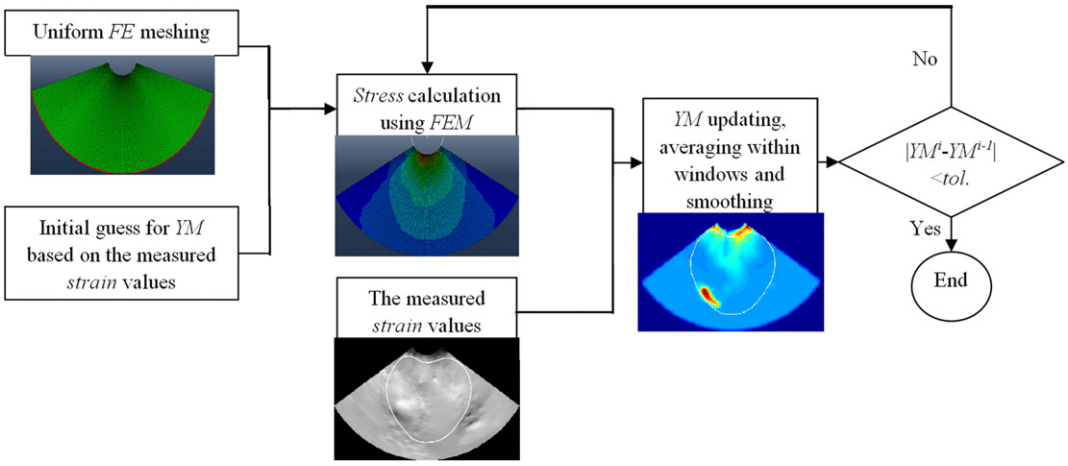

Figure 1. Flowchart illustrating the iterative procedure for YM reconstruction.

often leading to low image signal to noise (SNR) ratio. To improve strain imaging, full inversion-based elastography techniques were proposed [36]. Such techniques provide more accurate elasticity maps since they incorporate stress non-uniformity in the tissue elastic modulus image reconstruction. Despite the availability of theoretical and practical evidence pointing toward potentials of using this elastography technique for PCa detection and assessment, lack of clinical studies has hindered its consideration as a viable clinical tool. To our knowledge, there is no previous clinical study other than the study we performed to detect prostate lesions in two cases to obtain a proof of concept [37].

In this research, merits of the full-inversion-based prostate US elastography technique we developed recently [37] was investigated via a small pilot clinical study for the first time. Specifically, the efficacy of the technique was evaluated for detection and localization of prostate cancer and quantification of disease extent. Tumors identified using this technique were compared and correlated to those identified from the gold standard technique of whole-mount histopathology of prostatectomy specimens. Results show a good agreement between the reconstructed YM images and corresponding histopathology images in terms of tumor location within the prostate. They also demonstrate a good correlation between disease extent estimated from the reconstructed elasticity maps with those identified from histopathology images (r^2 = 0.71). This pilot study provides further evidence necessary to pave the way for clinical use of the proposed method aiming at early detection, localization and quantification of PCa as well as minimizing the number of prostate needle biopsies.

Table 1. Characteristics of the Patients

Pt. #	Age	PSA (ng/ml)	Gleason Score	Primary Gleason Component	Secondary Gleason Component	# of Lymph Nodes Examined	# of Lymph Nodes Involved	Stage of Primary Disease
1	74	7.1	9	4	5	6	1	pT3a
2	68	8	7	3	4	0	0	pT3a
3	68	6.4	9	4	5	4	1	pT3a
4	59	6.2	7	3	4	0	0	pT2
5	60	45.1	9	4	5	7	0	pT3a

Materials and Methods

Clinical Study Protocol and Data Collection

The clinical study was conducted in accordance with institutional research ethics approval from Sunnybrook Health Sciences Centre. The inclusion criteria were patients confirmed with adenocarcinoma of the prostate gland via a core biopsy procedure, having T2/T3 disease on histopathologic examination and consented for radical prostatectomy. Exclusion criteria were being on androgen deprivation therapy or prior chemotherapy or radiotherapy to the pelvis. All the ultrasound data in this study were collected based on standardized protocols of data acquisition. Ultrasound scans were performed with patients in lithotomy position using an in-house rail-based probe mount fixture. The ultrasonographer was blinded to the biopsy and histopathology results. Patients were scanned within 2 weeks before their radical prostatectomy. Data were collected with a Sonix RP system (Ultrasonix Medical Corporation, Richmond, BC, Canada) using a BPC8–4/10128 element curvilinear array ultrasound transducer at the tip of a biplane transrectal probe (Vermon S.A., Tours, France), with a center frequency of ~5 MHz. Collected data consisted of ultrasound B-mode images and RF data acquired in transverse planes spanning the whole prostate, prior to and after a quasi-static mechanical stimulation with the probe. RF data were sampled at 40 MHz. The applied line density was 512 with an 85% sector width permitting 430 RF lines per frame.

Histopathology Analysis

Following surgery, patient prostatectomy specimens were fixed, sectioned, and mounted on whole-mount histopathology slides (2" × 3"). The specimens were sectioned in a serial fashion from apex to base at a 90° orientation perpendicular to the urethra, nominally matching the orientation at which ultrasound scans were performed. Staining was performed with haematoxylin and eosin (H&E). Stained glass slides were digitized at 1-μm resolution using a confocal scanner (TISSUEscope; Huron Technologies, Waterloo, ON, Canada). The digital images were examined by a pathologist to detect and localize malignancies. Cancer regions were contoured by the pathologist on the images and their respective areas were quantified using ImageJ (NIH, Bethesda, MD, USA). The extent of disease was quantified by

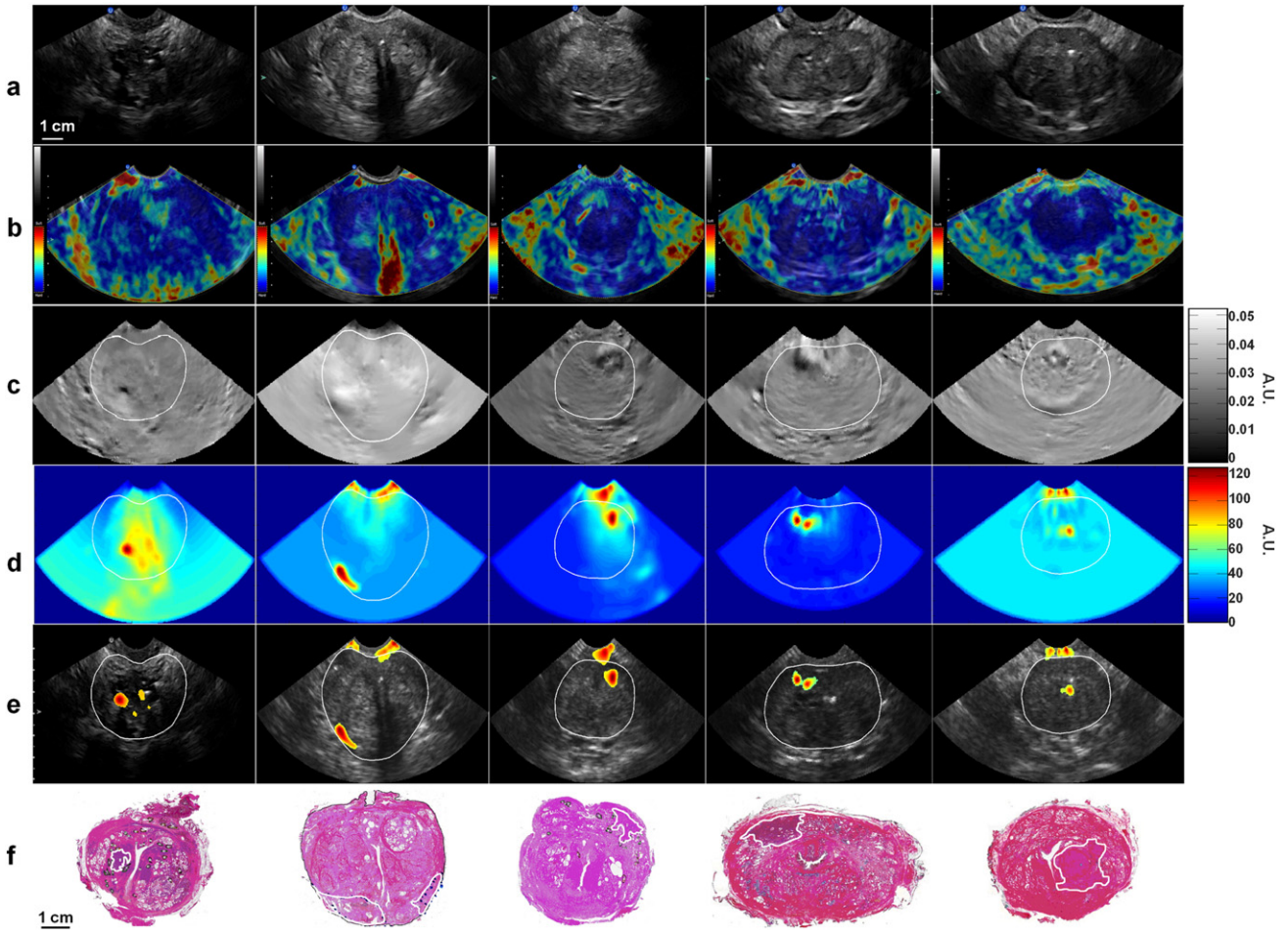

Figure 2. Imaging and histopathology data acquired from the 5 patients: (a) Ultrasound B-mode images (scale bar represents ~1 cm), (b) corresponding clinical strain images, (c) calculated strain images, (d) calculated YM images, (e) tumor regions based on YM images overlaid on the B-mode images, and (f) macroscopic images of whole-mount histopathology sections of the prostatectomy specimen (tumor region identified by pathologists are delineated with solid white contours; scale bar represents ~1 cm).

calculating the total area of contoured cancer regions in each prostate section relative to the area of the entire prostate in that section.

Young's Modulus (YM) Reconstruction

Because of the small deformation induced by TRUS probe's mechanical stimulation in the prostate, the prostate tissue can be considered as linear elastic and isotropic. Under these conditions, YM values can be calculated using the following equation derived from Hooke's law:

$$\frac{1}{E} = \frac{\varepsilon_{yy}}{\sigma_{yy} - \upsilon\sigma_{xx}} \tag{1}$$

In this equation ε and σ represent the tissue strain and stress resulting from mechanical stimulation, respectively, where x and y represent the two orthogonal axes of the strain image while υ is the tissue's Poisson's ratio. The prostate tissue can be considered as a near-incompressible material, hence $\upsilon = 0.49$ was employed for the YM image reconstruction.

To calculate strain values necessary for YM reconstruction, we used the method developed by Rivaz et al. [38,39]. In this method, strain values in the field of view are calculated using two radiofrequency (RF) signal sets corresponding to the pre- and post-compression states of the tissue.

In order to calculate the stress field in the prostate under the mechanical stimulation induced by the TRUS probe, finite element method (FEM) was used. FEM requires the geometry and YM values of the tissue as well as the boundary conditions. In this work, 2D TRUS B-mode images were used to construct the FE model. Since YM values are required for the FEM to calculate the stress values, the proposed method follows an iterative procedure. It starts with an initial guess of the YM values to calculate initial stress values followed by YM values updating in each iteration and continuing the iterations until convergence is achieved. The flow diagram of the proposed method is shown in Figure 1.

Statistical Analysis

In order to segment the tumor region in the YM images, YM values were normalized for each case to obtain the Z-scores of relative YM values. Areas with Z-cores >1.98 (having the top 5% stiffness) were then considered as the tumor region. The Dice similarity coefficient was used to evaluate the overlap between the tumor area determined by the proposed method and its counterpart identified in the corresponding histopathology image. Linear regression analysis

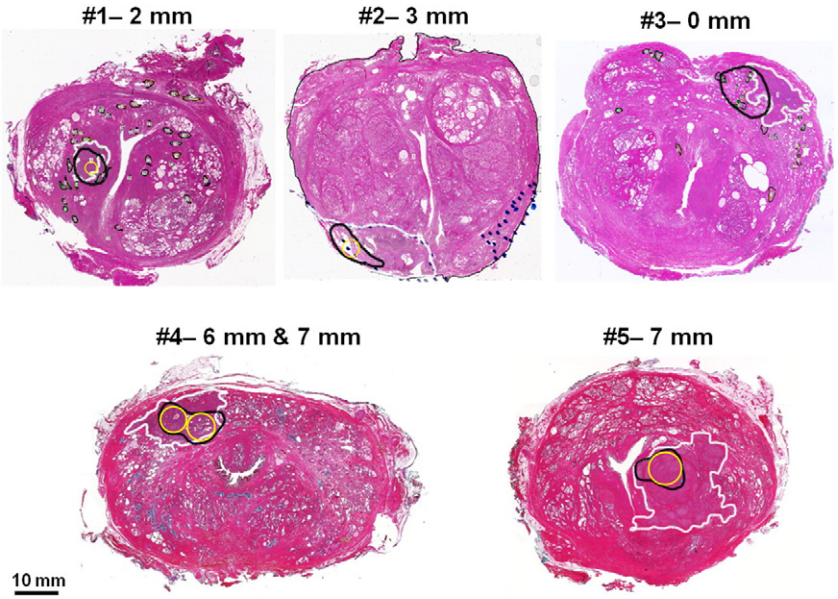

Figure 3. Registration of the tumor regions determined based on the YM images (outlined in solid black) to their corresponding histopathology images (with tumor regions outlined in solid white) for the 5 patients. Yellow outline in each case shows the biggest circle within respective overlap regions of black and white contours that is centered at the centroid of area contoured in black. The circle diameter is given for each case.

(PASW Statistics 18, SPSS Inc., Chicago, IL) was carried out to evaluate potential correlations between the extent of tumor identified on histopathology images and those determined noninvasively using the reconstructed YM images.

Results

Characteristics of the PCa patients who participated in this study, along with their disease specification, are summarized in Table 1. The patients' age ranged from 59 to 74 years with Average ± SD value of 66 ± 6 years. Their PSA level ranged from 6.2 to 45.1 ng/ml with Average ± SD value of 14.6 ± 17.1 ng/ml. Histopathology analysis indicated Gleason scores of 3 + 4 (40%) and 4 + 5 (60%) for the patients.

Figure 2 illustrates the B-mode images and their corresponding clinical strain images, calculated strain images, and the reconstructed YM images of the 5 patients. It also shows the tumor regions detected based on the YM images overlaid on the B-mode images as well as the histopathology image of each case. The tumor area is not quite detectable in B-mode and strain images due to low sensitivity/specificity and signal to noise ratio, whereas the YM images demonstrate the tumor areas quite clearly.

In order to calculate the Dice similarity coefficient for each case, the prostate was manually segmented in the respective US B-mode image and registered to the prostate contour in the corresponding histopathology image using a non-rigid registration function (B-spline grid, MATALB, The MathWorks Inc., Natick, MA, USA). The obtained transformation for each case was applied to the corresponding reconstructed YM image to be registered with the histology image. Figure 3 illustrates the tumor regions determined based on the YM images (outlined in solid black) registered to the histopathology images (with tumor regions outlined in solid white). Henceforth, the former and latter tumor outlines will be referred to as calculated and true tumor outlines, respectively. The Dice coefficients between these outlines were calculated at 0.74, 0.38, 0.26, 0.63 and 0.34 for the 5 patients, respectively. In addition to the true and calculated outlines of tumor, Figure 3 also shows circles outlined in yellow which are drawn to assess tumor targeting error in hypothetical utilization of the proposed technique in image-guided needle biopsy. For each case, the circle is centered at the centroid of the calculated tumor area while the radius was selected such that the circle remains within the overlap region of the true and calculated tumor areas.

As seen in the figure, in all patients except patients #3, the circles remain entirely within their respective common tumor areas. The radii of these circles range from 2 mm to 7 mm with Average ± SD

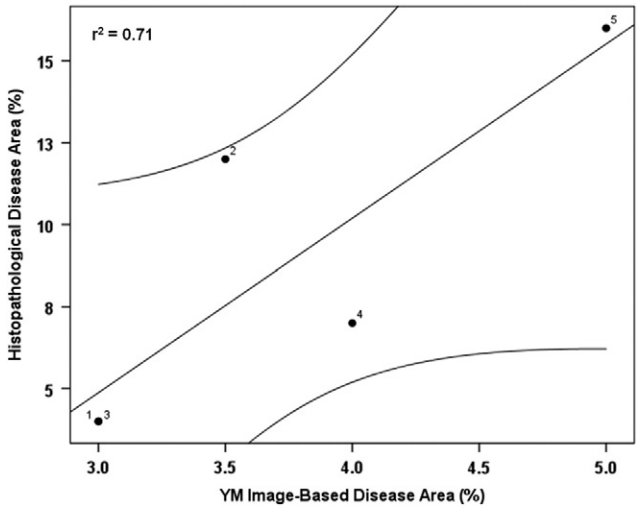

Figure 4. Extent of disease estimated/identified for each patient. The plot demonstrates relative areas of disease estimated noninvasively using the reconstructed YM images versus those identified from whole-mount histopathology. Each case has been labeled with the patient number. The lines were fitted to data via linear regression analyses and presented within the 95% confidence intervals.

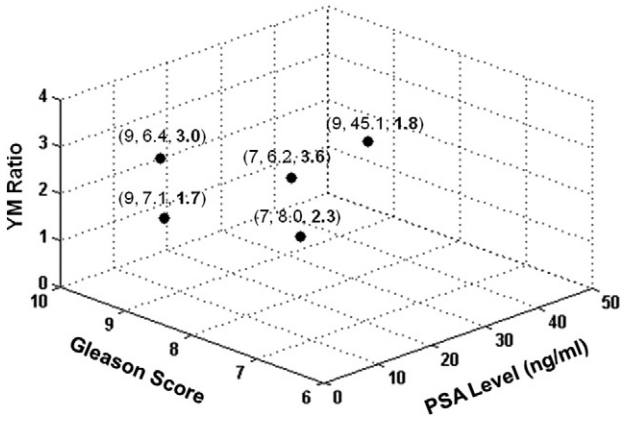

Figure 5. A three-dimensional scatter plot demonstrating relative YM of tumor to surrounding tissue versus Gleason score and PSA level for each patient. The numbers above each case present the corresponding Gleason score, PSA level, and YM ratio, respectively.

value of 5.0 ± 2.3 mm. This implies that by aiming at the centre of the calculated tumor area during needle biopsy guided by the proposed elastography technique, an average margin of targeting error of 5 mm is acceptable to hit the tumor. Figure 4 demonstrates results of linear regression analyses performed using the data obtained from all patients to evaluate the levels of correlation between the extent of disease predicted noninvasively using the reconstructed YM images and those identified from the whole-mount histopathology slides. Specifically, the scatter plot of predicted versus identified areas of disease relative to the whole prostate area is presented with the best line fitted to the data and the 95% confidence interval. Linear regression analysis resulted in an r^2 value of 0.71.

Figure 5 is a three-dimensional scatter plot demonstrating Gleason score versus corresponding PSA level and relative YM value associated with each tumor. The tumors demonstrated a 2.5 ± 0.8 folds higher stiffness on average compared to the surrounding normal tissues. No significant correlation was observed between the YM ratio of a tumor and its associated Gleason score or PSA level.

Discussion and Conclusions

In this pilot study, the efficacy of our proposed full inversion elastography method was investigated for detection, localization and quantification of prostate cancer using the data acquired from 5 patients. The objective of this preliminary clinical study was to evaluate our proposed elastography method for detection and localization of prostate lesion for PCa screening and needle biopsy guidance. The tumors were successfully detected in all cases based on their higher YM value compared to the surrounding tissue (average relative YM = 2.5 ± 0.8) in consistence with their available Gleason scores and PSA levels. On average, 76% ± 28% of the tumor regions detected based on the proposed method were inside tumor area identified within the histopathology images with 2 cases being entirely within their respective true tumor areas. The results indicate that there is a reasonably good correlation between tumor extension estimated using the proposed technique and its counterpart estimated from the gold standard findings of histopathology (r^2 = 0.71). This implies that YM images reconstructed using the proposed method are capable of estimating the extent of prostate cancer reasonably accurately. Overall, the results obtained in this preliminary pilot study suggest a good potential of the proposed method for detection and localization of prostate lesions as well as quantification of disease extent. The results are very encouraging, especially in the context of comparative assessment with what can be attained from traditional B-mode and strain images. Both of the latter options are known to have inadequate sensitivity/specificity and signal to noise ratio for detecting and localizing the tumor area.

The proposed elastography technique was evaluated for hypothetical utilization in image-guided needle biopsy procedures. The results indicated that in a needle biopsy procedure guided by the proposed technique, by aiming at the centre of the estimated tumor region, an average margin of targeting error of 5 mm is acceptable to hit the tumor. Conventional procedures for ultrasound-guided needle biopsy of prostate are not targeted as they involve randomly sampling distinct areas of prostate capsule [40]. Therefore, the proposed full inversion elastography technique can potentially facilitate a more accurate and targeted prostate needle biopsy procedure compared to conventional ultrasound-guided biopsy systems.

Although there is a good match between the tumor locations in the YM and histopathology images, the proposed method underestimated the extent of the disease in 3 cases out of the 5 cases investigated. Apart from YM reconstruction errors due to modeling and data acquisition and processing in addition to histopathology process errors, the observed underestimation implies incomplete consistency between cancer extent and tissue stiffening. In this regard, further research is required to investigate the stiffening process during prostate tumor formation to conceive better modeling tools for improved elastography algorithms [41]. Recent studies that used other imaging modalities including MRI to estimate the extent of prostate cancer reported that such imaging modalities also frequently underestimate the extent of disease [23,42]. Anwar et al. found that the margins of the tumor regions detected in MR images should be expanded at least by 5 mm to include 95% of actual tumor volume that was not initially covered [23].

Some of the YM images generated by the proposed method indicate some artifacts close to the rectum, near the probe. Due to the known intrinsic nonlinear elasticity nature of soft biological tissue, these areas are most likely due to the rectum tissue stiffening resulting from high strains applied at the contact area. Irrespective of their source, these artifacts were always outside the prostate capsule; therefore they are not a significant concern from clinical perspective.

The proposed elastography method generates quantitative maps of tissue biomechanical properties. As such, it has a good potential to be applied for lesion characterization. In the context of quantitative elastography, supersonic shear wave imaging was recently developed which has shown promise for imaging tissue elasticity [43]. Prostate clinical studies have demonstrated that Supersonic has sensitivity and specificity of 0.90 and 0.88 for prostate cancer characterization [44]. Although quantitative, the reproducibility of the Supersonic images is low [45] and the results are highly dependent to the operator [46]. The images are also heterogeneous and not suitable for tumor localization [46].

A number of other non-invasive imaging modalities have been investigated for PCa diagnosis including those based on PET and mp-MRI [47–50]. These imaging modalities are costly and frequently need external contrast agents to detect PCa. Ultrasound elastography is a relatively inexpensive and portable imaging modality that relies on the intrinsic biomechanical properties of tissues as the source of imaging contrast and, hence it does not require any exogenous contrast agents for imaging. It can be applied simultaneously with US

imaging to provide complementary information for PCa detection and characterization. An obstacle to using the proposed method for real-time YM imaging is the FE computation necessary for image reconstruction. This can be addressed effectively using model reduction techniques or parallel computing using graphics processing units (GPUs).

The clinical study presented in this work should be regarded as a preliminary pilot study to assess the potential accuracy and clinical utility of the proposed technique. To the best of our knowledge this is the first pilot clinical study of an unconstrained full-inversion-based US elastography technique. While it suffers from lack of high statistical power, it has shown significant promising results that warrants conducting a large clinical study involving a large cohort of patients with the aim of assessing the method's sensitivity and specificity.

In summary, the proposed quantitative elastography method investigated in this study has the potential to serve as a non-invasive, widely-available and low cost clinical tool for the detection localization and characterization of the prostate cancer. Based on the fact that PCa formation and degeneration introduce considerable alterations in tissue stiffness, the proposed method maybe potentially applied for evaluating cancer invasiveness as well as its response to anti-cancer therapies [51–53].

Acknowledgment

This work was supported by the Natural Sciences and Engineering Research Council of Canada (NSERC), the Terry Fox Foundation, and the Canadian Institutes of Health Research (CIHR).

References

[1] American Cancer Society (). www.cancer.org . [Accessed February 10, 2017].
[2] Presti JC (2000). Prostate cancer: assessment of risk using digital rectal examination, tumour grade, prostate-specific antigen, and systematic biopsy. *Radiol Clin North Am* **38**(1), 49–58.
[3] Salomon G, Kollerman J, Thederan I, Chun FKH, Budaus L, Schlomm T, Isbarn H, Heinzer H, Huland H, and Graefen M (2008). Evaluation of prostate cancer detection with ultrasound real-time elastography: A comparison with step section pathological analysis after radical prostatectomy. *J Eur Urol* **54**, 1354–1362.
[4] Shinohara K, Wheeler TM, and Scardino PT (1989). The appearance of prostate cancer on transrectal ultrasonography: correlation of imagining and pathological examinations. *Journal of Urology* **142**(1), 76–82.
[5] Carter HB, Hamper UM, Sheth S, Sanders RC, Epstein JI, and Walsh PC (1989). Evaluation of transrectal ultrasound in the diagnosis of prostate cancer. *J Urol* **142**, 1008–1010.
[6] Wink M, Frauscher F, Cosgrove D, Chapelon JY, Palwein L, Mitterberger M, Harvey C, Rouvière O, de la Rosette J, and Wijkstra H (2008). Contrast enhanced ultrasound and prostate cancer; a multicentre European research coordination project. *Eur Urol* **54**(5), 982–993.
[7] Feleppa E, Fair W, Tsai H, Porter C, Balaji K, Liu T, Kalisz A, Lizzi F, Rosado A, and Manolakis D (1999). Progress in two-dimensional and three dimensional ultrasonic tissue-type imaging of the prostate based on spectrum analysis and nonlinear classifiers. *Mol Urol* **3**, 303–310.
[8] Sadeghi-Naini A, Sofroni E, Papanicolau N, Falou O, Sugar L, Morton G, Yaffe MJ, Nam R, Sadeghian A, and Kolios MC, et al (2015). Quantitative ultrasound spectroscopic imaging for characterization of disease extent in prostate cancer patients. *Transl Oncol* **8**(1), 25–34.
[9] Simmons LA, Autier P, Zát'ura F, Braeckman J, Peltier A, Romic I, Stenzl A, Treurnicht K, Walker T, and Nir D, et al (2012). Detection, localisation and characterisation of prostate cancer by prostate HistoScanning™. *BJU Int* **110**(1), 28–35.
[10] Braeckman J, Autier P, Garbar C, Marichal MP, Soviany C, Nir R, Nir D, Michielsen D, Bleiberg H, and Egevad L, et al (2008). Computer-aided ultrasonography (HistoScanning): a novel technology for locating and characterizing prostate cancer. *BJU Int* **101**(3), 293–298.
[11] Javed S, Chadwick E, Edwards AA, Beveridge S, Laing R, Bott S, Eden C, and Langley S (2014). Does prostate HistoScanning™ play a role in detecting prostate cancer in routine clinical practice? Results from three independent studies. *BJU Int* **114**, 541–548.
[12] Schiffmann J, Tennstedt P, Fischer J, Tian Z, Beyer B, Boehm K, Sun M, Gandaglia G, Michl U, and Graefen M, et al (2014). Does HistoScanning™ predict positive results in prostate biopsy? A retrospective analysis of 1,188 sextants of the prostate. *World J Urol* **32**, 925–930.
[13] Beyersdorff D, Taupitz M, Winkelmann B, Fischer T, Lenk S, Loening SA, and Hamm B (2002). Patients with a history of elevated prostate-specific antigen levels and negative transrectal US-guided quadrant or sextant biopsy results: value of MR imaging. *Radiology* **224**(3), 701–706.
[14] Presti Jr JC, Hricak H, Narayan PA, Shinohara K, White S, and Carroll PR (1996). Local staging of prostatic carcinoma: comparison of transrectal sonography and endorectal MR imaging. *Am J Roentgenol* **166**(1), 103–108.
[15] Mullerad M, Hricak H, Kuroiwa K, Pucar D, Chen HN, Kattan MW, and Scardino PT (2005). Comparison of endorectal magnetic resonance imaging, guided prostate biopsy and digital rectal examination in the preoperative anatomical localization of prostate cancer. *Journal of Urology* **174**(6), 2158–2163.
[16] Turkbey B, Merino MJ, Gallardo EC, Shah V, Aras O, Bernardo M, Mena E, Daar D, Rastinehad AR, and Linehan WM, et al (2014). Comparison of endorectal coil and non-endorectal coil T2W and DW MRI at 3T for localizing prostate cancer: Correlation with whole-mount histopathology. *J Magn Reson Imaging* **39**(6), 1443–1448.
[17] Abd-Alazeez M, Kirkham A, Ahmed HU, Arya M, Anastasiadis E, Charman SC, Freeman A, and Emberton M (2014). Performance of multiparametric MRI in men at risk of prostate cancer before the first biopsy: a paired validating cohort study using template prostate mapping biopsies as the reference standard. *Prostate Cancer and Prostatic Disease* **17**(1), 40–46.
[18] Scheidler J, Hricak H, Vigneron DB, Yu KK, Sokolov DL, Huang LR, Zaloudek CJ, Nelson SJ, Carroll PR, and Kurhanewicz J (1999). Prostate cancer: localization with three-dimensional proton MR spectroscopic imaging-clinicopathologic study. *Radiology* **213**(2), 473–480.
[19] Brown G, Macvicar DA, Ayton V, and Husband JE (1995). The role of intravenous contrast enhancement in magnetic resonance imaging of prostatic carcinoma. *Clin Radiol* **50**(9), 601–606.
[20] Issa B (2002). In vivo measurement of the apparent diffusion coefficient in normal and malignant prostatic tissues using echoplanar imaging. *J Magn Reson Imaging* **16**(2), 196–200.
[21] Akin O, Sala E, Moskowitz CS, Kuroiwa K, Ishill NM, Pucar D, Scardino PT, and Hricak H (2006). Transition zone prostate cancers: features, detection, localization, and staging at endorectal MR imaging. *Radiology* **239**, 784–792.
[22] Yoshizako T, Wada A, Hayashi T, Uchida K, Sumura M, Uchida N, Kitagaki H, and Igawa M (2008). Usefulness of diffusion-weighted imaging and dynamic contrast-enhanced magnetic resonance imaging in the diagnosis of prostate transition-zone cancer. *Acta Radiol* **49**(10), 1207–1213.
[23] Anwar M, Westphalen AC, Jung AJ, Noworolski SM, Simko JP, Kurhanewicz J, Roach III M, Carroll PR, and Coakley FV (2014). Role of endorectal MR imaging and MR spectroscopic imaging in defining treatable intraprostatic tumor foci in prostate cancer: Quantitative analysis of imaging contour compared to whole-mount histopathology. *Radiother Oncol* **110**(2), 303–308.
[24] Steenbergen P, Haustermans K, Lerut E, Oyen R, De Wever L, Van den Bergh L, Kerkmeijer LG, Pameijer FA, Veldhuis WB, and van der Voort van Zyp JR, et al (2015). Prostate tumor delineation using multiparametric magnetic resonance imaging: Inter-observer variability and pathology validation. *Radiother Oncol* **115**(2), 186–190.
[25] Liu IJ, Zafar MB, Lai Y-H, Segall GM, and Terris MK (2001). Fluorodeoxyglucose positron emission tomography studies in diagnosis and staging of clinically organ-confined prostate cancer. *Urology* **57**(1), 108–111.
[26] Effert PJ, Bares R, Handt S, Wolff JM, Büll U, and Jakse G (1996). Metabolic imaging of untreated prostate cancer by positron emission tomography with 18fluorine-labeled deoxyglucose. *Journal of Urology* **155**(3), 994–998.
[27] Hossein J (2012). Molecular imaging of prostate cancer: PET radiotracers. *AJR Am J Roentgenol* **199**(2), 278–291.
[28] Sarkar S and Das S (2016). A review of imaging methods for prostate cancer detection. *Biomed Eng Comput Biol* **7**(Suppl. 1), 1–15.
[29] Fung YC (1981.). Biomechanical properties of living tissue. New York: Springer Verlag; 1981.
[30] Anderson WAD (1953.). Pathology. St. Louis: C. V. Mosby Co.; 1953.

[31] Zhang M, Nigwekar P, Castaneda B, Hoyt K, Joseph JV, Agnes A, Messing EEM, Strang JG, Rubens DJ, and Parker KJ (2008). Quantitative characterization of viscoelastic properties of human prostate correlated with histology. *Ultrasound in Med & Biol* **34**(7), 1033–1042.

[32] Miyanaga N, Akaza H, Yamakawa M, Oikawa T, Sekido N, Hinotsu S, Kawai K, Shimazui T, and Shiina T (2006). Tissue elasticity imaging for diagnosis of prostate cancer: a preliminary report. *Int J Urol* **13**(12), 1514–1518.

[33] Pallwein L, Mitterberger M, Gradl J, Aigner F, Horninger W, Strasser H, Bartsch G, zur Nedden D, and Frauscher F (2007). Value of contrast-enhanced ultrasound and elastography in imaging of prostate cancer. *Curr Opin Urol* **17**(1), 39–47.

[34] König K, Scheipers U, Pesavento A, Lorenz A, Ermert H, and Senge T (2005). Initial experiences with real-time elastography with real-time elastography guided biopsies of the prostate. *J Urol* **174**(1), 115–117.

[35] Pallwein L, Mitterberger M, Struve P, Horninger W, Aigner F, Bartsch G, Gradl J, Schurich M, Pedross F, and Frauscher F (2007). Comparison of sonoelastography guided biopsy with systematic biopsy: impact on prostate cancer detection. *Eur Radiol* **17**(9), 2278–2285.

[36] Samani A, Bishop J, and Plewes DB (2001). A constrained modulus reconstruction technique for breast cancer assessment. *IEEE Trans Medical Imaging* **20**(9), 877–885.

[37] Mousavi SR, Sadeghi-Naini A, Czarnota JG, and Samani A (2014). Towardsclinical prostate ultrasound elastography using full inversion approach. *Med Phys* **41**(3) [033501; 12 pp.].

[38] Rivaz H, Boctor E, Choti M, and Hager G (2011). Real-time regularized ultrasound elastography. *IEEE TMI* **30**, 928–945.

[39] Rivaz H, Boctor E, Foroughi P, Zellars R, Fichtinger G, and Hager G (2008). Ultrasound elastography: a dynamic programming approach. *IEEE TMI* **27**, 1373–1377.

[40] Yacoub JH, Verma S, Moulton JS, Eggener S, and Aytekin O (2012). Imaging-guided prostate biopsy: conventional and emerging techniques. *Radiographics* **32**(3), 819–837.

[41] Cox TR and Erler JT (2011). Remodeling and homeostasis of the extracellular matrix: implications for fibrotic diseases and cancer. *Dis Model Mech* **4**(2), 165–178.

[42] Gibson E, Bauman GS, Romagnoli C, Cool DW, Bastian-Jordan M, Kassam Z, Gaed M, Moussa M, Gómez JA, and Pautler SE, et al (2016). Toward prostate cancer contouring guidelines on magnetic resonance imaging: dominant lesion gross and clinical target volume coverage via accurate histology fusion. *International Journal of Radiation Oncology Biology Physics* **96**(1), 188–196.

[43] Bercoff J, Tanter M, and Fink M (2004). Supersonic shear imaging: A new technique for soft tissue elasticity mapping. *IEEE Trans Ultrason Ferroelectr Freq Control* **51**(4), 396–409.

[44] Ahmad S, Cao R, Varghese T, Bidaut L, and Nabi G (2013). Transrectal quantitative shear wave elastography in the detection and characterisation of prostate cancer. *Surg Endoscopy* **27**(9), 3280–3287.

[45] Ramnarine KV, Garrard JW, Kanber B, Nduwayo S, Hartshorne TC, and Robinson TG (2014). Shear wave elastography imaging of carotid plaques: feasible, reproducible and of clinical potential. *Cardiovasc Ultrasound* **12**, 49.

[46] Woo S, Kim SY, Cho JY, and Kim SH (2014). Shear wave elastography for detection of prostate cancer: A preliminary study. *Korean J Radiol* **15**(3), 346–355.

[47] Kelloff GJ, Choyke P, and Coffey DS (2009). Challenges in clinical prostate cancer: role of imaging. *AJR Am J Roentgenol* **192**, 1455–1470.

[48] Röthke MC, Afshar-Oromieh A, and Schlemmer HP (2013). Potential of PET/MRI for diagnosis of prostate cancer. *Radiologe* **53**, 676–681.

[49] Turkbey B, Mena E, Aras O, Garvey B, Grant K, and Choyke PL (2013). Functional and molecular imaging: applications for diagnosis and staging of localised prostate cancer. *Clin Oncol* **25**, 451–460.

[50] Mari Aparici C and Seo Y (2012). Functional imaging for prostate cancer: therapeutic implications. *Semin Nucl Med* **42**, 328–342.

[51] Sadeghi-Naini A, Falou O, Hudson JM, Bailey C, Burns PN, Yaffe MJ, Stanisz GJ, Kolios MC, and Czarnota GJ (2012). Imaging innovations for cancer therapy response monitoring. *Imaging Med* **4**, 311–327.

[52] Falou O, Sadeghi-Naini A, Prematilake S, Sofroni E, Papanicolau N, Iradji S, Jahedmotlagh Z, Lemon-Wong S, Pignol JP, and Rakovitch E, et al (2013). Evaluation of neoadjuvant chemotherapy response in women with locally advanced breast cancer using ultrasound elastography. *Transl Oncol* **6**, 17–24.

[53] Sannachi L, Tadayyon H, Sadeghi-Naini A, Tran W, Gandhi S, Wright F, Oelze M, and Czarnota GJ (2014). Non-invasive evaluation of breast cancer response to chemotherapy using quantitative ultrasonic backscatter parameters. *Med Image Anal* **20**(1), 224–236.